Phase locking and multistability in the topological Kuramoto model on cell complexes

Iva Bačić [1, 2, *] Michael T. Schaub [3] Jürgen Kurths [4] and Dirk Witthaut [1, 5]

[1]*Institute of Climate and Energy Systems: Energy Systems Engineering (ICE-1),*
Forschungszentrum Jülich, 52428 Jülich, Germany
[2]*Institute of Physics Belgrade, University of Belgrade, Serbia*
[3]*RWTH Aachen University, Aachen, Germany*
[4]*Potsdam Institute for Climate Impact Research (PIK), Potsdam, Germany*
[5]*Institute for Theoretical Physics, University of Cologne, 50937 Köln, Germany*

The topological Kuramoto model generalizes classical synchronization models by including higher-order interactions, with oscillator dynamics defined on cells of arbitrary dimension within simplicial or cell complexes. In this article, we demonstrate multistability in the topological Kuramoto model and develop the topological nonlinear Kirchhoff conditions algorithm to identify all phase-locked states on arbitrary cell complexes. The algorithm is based on a generalization of Kirchhoff's laws to cell complexes of arbitrary dimension and nonlinear interactions between cells. By applying this framework to rings, Platonic solids, and simplexes, as minimal representative motifs of larger networks, we derive explicit bounds (based on winding number constraints) that determine the number of coexisting stable states. We uncover structural cascades of multistability, inherited from both lower and higher dimensions and demonstrate that cell complexes can generate richer multistability patterns than simplicial complexes of the same dimension. Moreover, we find that multistability patterns in cell complexes appear to be determined by the number of boundary cells, hinting a possible universal pattern.

I. INTRODUCTION

From neuronal activity to power grid operation, synchronization phenomena are a hallmark of many natural and engineered systems [1, 2]. For such systems, the Kuramoto model of coupled oscillators has served as a prototypical model for understanding how synchronization emerges from local interactions [3, 4]. While early studies focused on globally coupled systems [5], later work extended the model to complex networks, revealing that network topology plays a crucial role in determining the onset and nature of synchronization [6]. Such systems often exhibit multistability, where multiple distinct synchronized states can coexist [7–10].

In their classical form, the coupling between the oscillators is pairwise. This assumption is valid for many systems, but in various contexts, such as neuronal assemblies [11], the brain connectome [12–14] multimode lasers, [15], or protein interaction networks [16], it is likely too restrictive to capture all the relevant couplings in the system. Group interactions, encoded by higher-order connectivity structures, are increasingly recognized as being crucial to many collective dynamics [17–22]. A variety of recent advances in network science [12–14, 18, 19, 23–28] have introduced models where the dynamics is not defined only on nodes, but also lives on edges, faces, or higher-dimensional elements of simplicial or cell complexes. The topological Kuramoto model [29–32] is among the most prominent dynamical models in this framework, revealing universal features absent in conventional networks, such as abrupt synchronization

transitions [33, 34] or topologically-induced synchronization obstructions [35, 36]. While some aspects of multistability [37, 38] and phase locking [32] in the topological Kuramoto model have been analyzed separately, there is a lack of systematic frameworks to analyse how multistable phase-locked states can arise from higher-order interactions.

To bridge this gap, here we investigate phase locking and multistability in the topological Kuramoto model defined on general cell complexes. Unlike earlier works which employ the master stability function formalism to study synchronization in this model [36, 39, 40], we propose the topological nonlinear Kirchhoff conditions algorithm, which may be seen as a generalization of Kirchhoff's current and voltage laws. Moreover, thus far most studies have focused on simplicial complexes. Yet many real-world structures, such as architectural trusses, social interactions or protein complexes, are better described as cell complexes [41–44], which consist of larger polyhedral faces. Despite their prevalence, the study of dynamical phenomena on cell complexes is still in its infancy.

Our novel algorithm systematically identifies distinct phase-synchronized states in cell complexes, and allows us to define rigorous criteria for when going beyond pairwise interactions pays off in terms of multistability. We demonstrate our approach on three minimal but paradigmatic classes of cell complexes: (i) rings, (ii) Platonic solids, and (iii) simplexes. These basic motifs can be combined to build larger complexes with potentially even richer multistability. Our framework can be applied to any cell complex and any dimension. For simplicity, however, we focus here on dynamics supported on edges, with interactions mediated through nodes and faces (2-simplices). This case is moreover particularly relevant to applications (see, e.g., Ref. [43] and references therein).

* i.bacic@fz-juelich.de

Our main findings are:

- Cell complexes can support richer multistability than simplicial complexes of the same dimension. This extends previous results on their enhanced synchronizability [36].

- Higher-order connectivity can result in *structural cascades of multistability*, which involve sequences of stable states inherited from both lower and higher dimensions. The number of stable states increases with system size and arises from winding-number bounds determined by the cell boundaries.

- We find indications of possible *universality patterns*: different complexes, such as dual Platonic solids, have the same multistability patterns if they share certain structure-dependent parameters, related to the number of boundary cells in the upper and lower dimension.

Our results show how higher-order topology governs synchronization and the emergence of multistability, revealing new mechanisms for collective behavior in complex systems with non-pairwise interactions.

II. CELL COMPLEXES

Cell complexes are generalised network structures that contain cells of different dimensions [12, 41, 42]. In addition to nodes ($n = 0$) and edges ($n = 1$) found in standard graphs, they can include polygons ($n = 2$), polytopes ($n = 3$) and other higher-dimensional elements. Most studies on synchronization focus on the special case of simplicial complexes [29, 32], where each cell is an Euclidean simplex, but many real-world systems are better described by cell complexes.

The boundary of an n-dimensional cell consists of a number of cells of dimension $n - 1$, and cells of consecutive dimensions are linked by boundary operators. We denote a set of cells of dimension n by $S_{[n]}$, with $N_{[n]} = |S_{[n]}|$. We generally consider a complex of cells $S_{[n-1]}$, $S_{[n]}$, $S_{[n+1]}$, where each boundary of a cell in $S_{[n']}$ must be an element of $S_{[n'-1]}$ for every n'. For calculations, we introduce an algebraic representation where we label all cells $j \in S_{[n]}$ consecutively as $j = 1, 2, \ldots, N_{[n]}$ and represent each cell by the jth standard unit vector $\boldsymbol{u}_j \in \mathbb{R}^{N_{[n]}}$. Fixing an orientation of each cell, we can represent the boundary operator between $S_{[n]}$ and $S_{[n-1]}$ by a matrix $\boldsymbol{B}_{[n]} \in \mathbb{R}^{N_{[n-1]} \times N_{[n]}}$ with entries $+1$, -1 or 0.

We briefly recall several important properties of the boundary matrices. First, the boundary of a boundary is always empty, such that

$$\boldsymbol{B}_{[n]}\boldsymbol{B}_{[n+1]} = 0, \qquad \boldsymbol{B}_{[n+1]}^\top \boldsymbol{B}_{[n]}^\top = 0. \qquad (1)$$

Using this property, one can show that every vector $\boldsymbol{x}_{[n]} \in \mathbb{R}^{N_{[n]}}$ can be decomposed according to the Hodge

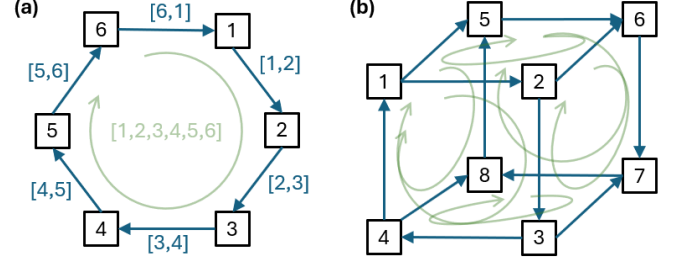FIG. 1. Two examples of cell complexes for $n = 1$. Nodes are colored in black, edges in blue and faces in light green.

decomposition [45] as

$$\boldsymbol{x}_{[n]} = \boldsymbol{x}_{[n]}^H + \boldsymbol{B}_{[n]}^\top \boldsymbol{z}_{[n-1]} + \boldsymbol{B}_{[n+1]} \boldsymbol{z}_{[n+1]}, \qquad (2)$$

where $\boldsymbol{x}_{[n]}^H$ is referred to as the harmonic component that satisfies $\boldsymbol{B}_{[n+1]}^\top \boldsymbol{x}_{[n]}^H = \boldsymbol{0}$ and $\boldsymbol{B}_{[n]}\boldsymbol{x}_{[n]}^H = \boldsymbol{0}$. This decomposition plays a central role in our analysis.

To study dynamics defined on such cell complexes, we define *phase* variables supported on n-dimensional cells. These phases are coupled via interactions occurring "from below" via $(n - 1)$-dimensional boundaries and "from above", via the $(n+1)$-dimensional cells. For example, for $n = 1$, edges can interact if they share a node, or if they are part of the same polygonal face. Two illustrative examples are shown in Fig. 1. The first is a hexagon, whose boundary consists of six edges ($n = 1$), each of which has a boundary of two nodes ($n = 0$). The second is a cube, with boundaries consisting of the six faces ($n = 2$), 12 edges ($n = 1$) and 8 nodes ($n = 0$). Ordinary graphs are recovered for $n = 0$, where only pairwise interactions exist. Including group interactions in cell complexes with $n \geq 1$ allows one to describe a much richer variety of dynamical systems.

III. PHASE LOCKING IN THE TOPOLOGICAL KURAMOTO MODEL

In this article we consider a generalized topological Kuramoto model allowing for inhomogeneous coupling constants. The basic dynamic variables are the phases $\theta_i(t)$ associated to each n-dimensional cell. These phases interact via cells of lower and higher dimension. In the case $n = 1$ for example, phases are defined for each edge, and interact via vertices and faces. Summarizing the dynamical variables in the vector $\boldsymbol{\theta} = \left(\theta_1, \ldots \theta_{N_{[n]}}\right)^\top$, the equations of motion read

$$\frac{d\boldsymbol{\theta}}{dt} = \boldsymbol{\omega} - \boldsymbol{B}_{[n]}^\top \boldsymbol{K}_{[n]} \sin\left(\boldsymbol{B}_{[n]}\boldsymbol{\theta}\right)$$
$$- \boldsymbol{B}_{[n+1]}\boldsymbol{K}_{[n+1]} \sin\left(\boldsymbol{B}_{[n+1]}^\top \boldsymbol{\theta}\right), \qquad (3)$$

where $\boldsymbol{\omega}$ is the vector of the natural frequencies. The matrices $\boldsymbol{K}_{[n]}$ and $\boldsymbol{K}_{[n+1]}$ are diagonal and summarize

positive coupling constants. In the case $n = 0$ the coupling constants correspond to edge weights. The original topological Kuramoto model is recovered by setting $\boldsymbol{K}_{[n]} = \sigma \mathbb{1}$ and $\boldsymbol{K}_{[n+1]} = \sigma \mathbb{1}$, where $\mathbb{1}$ is the identity matrix of the respective size. The standard Kuramoto model for weighted complex networks is recovered for $n = 0$, with no interaction via the lower dimension.

We can decouple the dynamics by multiplying the equations of motion by $\boldsymbol{B}_{[n]}$ and $\boldsymbol{B}_{[n+1]}^\top$ from the left [29]. Defining the variables

$$\boldsymbol{\theta}^{[+]} = \boldsymbol{B}_{[n+1]}^\top \boldsymbol{\theta}, \quad \text{and} \quad \boldsymbol{\theta}^{[-]} = \boldsymbol{B}_{[n]}\boldsymbol{\theta}, \tag{4}$$

we obtain the decoupled equations

$$\frac{d\boldsymbol{\theta}^{[+]}}{dt} = \boldsymbol{B}_{[n+1]}^\top \boldsymbol{\omega} - \boldsymbol{L}_{[n+1]}^{[down]} \boldsymbol{K}_{[n+1]} \sin\left(\boldsymbol{\theta}^{[+]}\right) \tag{5}$$

$$\frac{d\boldsymbol{\theta}^{[-]}}{dt} = \boldsymbol{B}_{[n]}\boldsymbol{\omega} - \boldsymbol{L}_{[n-1]}^{[up]} \boldsymbol{K}_{[n]} \sin\left(\boldsymbol{\theta}^{[-]}\right) \tag{6}$$

with the Laplacian matrices

$$\boldsymbol{L}_{[n-1]}^{[up]} = \boldsymbol{B}_{[n]}\boldsymbol{B}_{[n]}^\top, \qquad \boldsymbol{L}_{[n+1]}^{[down]} = \boldsymbol{B}_{[n+1]}^\top \boldsymbol{B}_{[n+1]}. \tag{7}$$

Here, we analyze the phase locked states of the topological Kuramoto model. Setting the time derivatives to zero, we get the conditions

$$\boldsymbol{B}_{[n+1]}^\top \boldsymbol{\omega} = \boldsymbol{L}_{[n+1]}^{[down]} \boldsymbol{K}_{[n+1]} \sin\left(\boldsymbol{\theta}^{[+]}\right) \tag{8}$$

$$\boldsymbol{B}_{[n]}\boldsymbol{\omega} = \boldsymbol{L}_{[n-1]}^{[up]} \boldsymbol{K}_{[n]} \sin\left(\boldsymbol{\theta}^{[-]}\right). \tag{9}$$

The stability of phase locking can be determined from the Jacobian matrix of the equations of motion (3) given by

$$\boldsymbol{J} = -\boldsymbol{B}_{[n]}^\top \boldsymbol{K}_{[n]} \mathrm{diag}\left[\cos\left(\boldsymbol{\theta}^{[-]}\right)\right]\boldsymbol{B}_{[n]}$$
$$- \boldsymbol{B}_{[n+1]}\boldsymbol{K}_{[n+1]}\mathrm{diag}\left[\cos\left(\boldsymbol{\theta}^{[+]}\right)\right]\boldsymbol{B}_{[n+1]}^\top. \tag{10}$$

In general, a stationary state is linearly stable if the real part of all eigenvalues is negative [46]. If the stationary state satisfies the conditions

$$\cos\left(\boldsymbol{\theta}^{[-]}\right) > 0 \quad \text{and} \quad \cos\left(\boldsymbol{\theta}^{[+]}\right) > 0 \tag{11}$$

we find that all eigenvalues are real and satisfy the following conditions: (i) If an eigenvector $\boldsymbol{v}$ is purely harmonic, then the associated eigenvalue is given by $\lambda = 0$. (ii) If an eigenvector $\boldsymbol{v}$ is not purely harmonic, then the associated eigenvalue satisfies $\lambda < 0$. A proof is given in appendix A. We thus conclude that a stationary state that satisfies Eq. (11) is linearly stable with respect to perturbations that are orthogonal to the harmonic subspace and neutrally stable with respect to harmonic perturbations. Since harmonic perturbations do not affect the projected quantities $\boldsymbol{\theta}^{[+]}$ and $\boldsymbol{\theta}^{[-]}$, phase locking is linearly stable.

In the following we will mainly concentrate on phase locked states that satisfy the conditions in Eq. (11) and

refer to them as normal fixed points. Stationary states that violate Eq. (11) are typically, but not always, linearly unstable. For the ordinary Kuramoto model $n = 0$, it has been shown that stable phase locked states that violate these conditions exist at the border of the stability region [47]. We will return to this question in Sec. V, Fig. 2, in the context of polygonal face complexes, where we find such stable phase-locked states that aren't normal fixed points.

IV. PHASE LOCKING AND MULTISTABILITY

Next, we introduce a two-step approach to explore phase locking: In the first step, we generate a space of solution candidates determined by a linear set of equations. In the second step, the actual solutions are singled out by a nonlinear condition. These two steps generalize Kirchhoff's current law and Kirchhoff's voltage law from circuits theory, as we will discuss in detail below.

We first define the auxiliary variables

$$\boldsymbol{\psi}^{[\pm]} = \sin\left(\boldsymbol{\theta}^{[\pm]}\right). \tag{12}$$

In the case $n = 1$, the original dynamical variables $\boldsymbol{\theta}$ are defined on the edges of the cell complex, while the variables $\boldsymbol{\psi}^{[+]}$ are defined on the faces, and the variables $\boldsymbol{\psi}^{[-]}$ on the nodes. In the case $n = 0$, the original dynamical variables $\boldsymbol{\theta}$ are defined on the nodes of the graph, while the auxiliary variables $\boldsymbol{\psi}^{[+]}$ are defined on its edges. In the theory of supply networks, the entries of $\boldsymbol{K}_{[1]}\boldsymbol{\psi}^{[+]}$ are interpreted as flows [48–50].

We then construct the solution candidates in terms of the auxiliary variables. The equations (9) read

$$\boldsymbol{B}_{[n+1]}^\top \boldsymbol{\omega} = \boldsymbol{L}_{[n+1]}^{[down]} \boldsymbol{K}_{[n+1]} \boldsymbol{\psi}^{[+]} \tag{13}$$

$$\boldsymbol{B}_{[n]}\boldsymbol{\omega} = \boldsymbol{L}_{[n-1]}^{[up]} \boldsymbol{K}_{[n]} \boldsymbol{\psi}^{[-]}. \tag{14}$$

If we treat the $\boldsymbol{\psi}^{[\pm]}$ as free variables, the solutions to this linear set of Eqs. (13) and (14) define a low-dimensional affine linear subspace.

To parametrize the set of solution candidates, we need the kernel of the matrices $\boldsymbol{B}_{[n+1]}$ and $\boldsymbol{B}_{[n]}^\top$. We compute a basis of these kernels and store the basis vectors as columns of the matrices $\boldsymbol{C}_{[n+1]}$ and $\boldsymbol{C}_{[n]}^\top$, respectively. We thus have

$$\boldsymbol{B}_{[n+1]}\boldsymbol{C}_{[n+1]} = \boldsymbol{0}, \qquad \boldsymbol{B}_{[n]}^\top \boldsymbol{C}_{[n]}^\top = \boldsymbol{0}. \tag{15}$$

Note that these matrices are intimately related, but not identical to the matrices $\boldsymbol{B}_{[n+2]}$ and $\boldsymbol{B}_{[n-1]}^\top$ via Eq. (1). The columns of the matrix $\boldsymbol{B}_{[n+2]}$ ($\boldsymbol{B}_{[n-1]}^\top$) lie in the kernel of $\boldsymbol{B}_{[n+1]}$ ($\boldsymbol{B}_{[n]}^\top$), but the kernel also contains the harmonic vectors. Having constructed the kernel, we can write the solutions of Eqs. (13) and (14) as

$$\boldsymbol{\psi}^{[+]} = \boldsymbol{\psi}_{\mathrm{sp}}^{[+]} + \boldsymbol{K}_{[n+1]}^{-1}\boldsymbol{C}_{[n+1]}\boldsymbol{\zeta}^{[+]},$$
$$\boldsymbol{\psi}^{[-]} = \boldsymbol{\psi}_{\mathrm{sp}}^{[-]} + \boldsymbol{K}_{[n]}^{-1}\boldsymbol{C}_{[n]}^\top \boldsymbol{\zeta}^{[-]}, \tag{16}$$

where $\boldsymbol{\zeta}^{[\pm]}$ are vectors of free coefficients which parametrize the homogeneous solution space, such that different choices of $\boldsymbol{\zeta}^{[\pm]}$ provide different candidate solutions. The particular solutions $\boldsymbol{\psi}_{\mathrm{sp}}^{[\pm]}$ can be calculated by applying the Moore–Penrose pseudoinverse to Eqs. (13)-(14) such that

$$\boldsymbol{\psi}_{\mathrm{sp}}^{[+]} = \left(\boldsymbol{L}_{[n+1]}^{[down]}\boldsymbol{K}_{[n+1]}\right)^{\dagger}\boldsymbol{B}_{[n+1]}^{\top}\boldsymbol{\omega} = \boldsymbol{K}_{[n+1]}^{-1}\boldsymbol{B}_{[n+1]}^{\dagger}\boldsymbol{\omega}$$

$$\boldsymbol{\psi}_{\mathrm{sp}}^{[-]} = \left(\boldsymbol{L}_{[n-1]}^{[up]}\boldsymbol{K}_{[n]}\right)^{\dagger}\boldsymbol{B}_{[n]}\boldsymbol{\omega} = \boldsymbol{K}_{[n]}^{-1}\boldsymbol{B}_{[n]}^{\dagger\top}\boldsymbol{\omega} \qquad (17)$$

This corresponds to the least squares solution of the linear system given by Eqs. (13)- (14).

Therefore, $\psi^{[\pm]} = 0$ if $\boldsymbol{\omega} = 0$. Furthermore, the auxiliary variables must satisfy the inequalities

$$|\boldsymbol{\psi}^{[\pm]}| \leq 1, \qquad (18)$$

since all variables are defined via sine functions. Hence, the set of solution candidates is given by the intersections of a low dimensional affine subspace and the unit cube. The intersection can be empty depending on $\boldsymbol{\omega}$.

The complexity of finding a stationary state is then shifted to the question of whether a solution candidate (16) exists that can be expressed as (12). To approach this topic, we first discuss how to recover the original variables $\boldsymbol{\theta}^{[\pm]}$ from the $\boldsymbol{\psi}^{[\pm]}$. If the equations Eq. (12) have solutions, they can have the form $\arcsin(\cdot)$ or $\pi - \arcsin(\cdot)$. To keep track of the two options, we partition the set of cells as follows:

$$S_{[n+1]}^{\bullet} = \left\{j \in S_{[n+1]} \,\middle|\, \cos\left(\theta_j^{[+]}\right) > 0\right\}$$
$$S_{[n+1]}^{\circ} = S_{[n+1]}\backslash S_{[n+1]}^{\bullet}$$
$$S_{[n-1]}^{\bullet} = \left\{i \in S_{[n-1]} \,\middle|\, \cos\left(\theta_i^{[-]}\right) > 0\right\}$$
$$S_{[n-1]}^{\circ} = S_{[n-1]}\backslash S_{[n-1]}^{\bullet}. \qquad (19)$$

We can now consistently express $\boldsymbol{\theta}^{[\pm]}$ in terms of $\boldsymbol{\psi}^{[\pm]}$, having in mind the definitions in Eq. (12),

$$j \in S_{[n+1]}^{\bullet} : \left(\boldsymbol{B}_{[n+1]}^{\top}\boldsymbol{\theta}\right)_j = f_+\left(\psi_j^{[+]}\right) = \arcsin\left(\psi_j^{[+]}\right)$$
$$j \in S_{[n+1]}^{\circ} : \left(\boldsymbol{B}_{[n+1]}^{\top}\boldsymbol{\theta}\right)_j = f_-\left(\psi_j^{[+]}\right) = \pi - \arcsin\left(\psi_j^{[+]}\right)$$
$$i \in S_{[n-1]}^{\bullet} : \left(\boldsymbol{B}_{[n]}\boldsymbol{\theta}\right)_i = f_+\left(\psi_i^{[-]}\right) = \arcsin\left(\psi_i^{[-]}\right)$$
$$i \in S_{[n-1]}^{\circ} : \left(\boldsymbol{B}_{[n]}\boldsymbol{\theta}\right)_i = f_-\left(\psi_i^{[-]}\right) = \pi - \arcsin\left(\psi_i^{[-]}\right) \qquad (20)$$

up to integer multiples of 2π. We summarize these components in the two vector-valued functions $\boldsymbol{f}_{[n+1]}(\boldsymbol{\psi}^{[+]})$ and $\boldsymbol{f}_{[n-1]}(\boldsymbol{\psi}^{[-]})$.

The question whether a solution candidate (16) exists that can be expressed as (12) can thus be formulated as

$$\boldsymbol{f}_{[n+1]}(\boldsymbol{\psi}^{[+]}) \in \mathrm{image}\left(\boldsymbol{B}_{[n+1]}^{\top}\right),$$
$$\boldsymbol{f}_{[n-1]}(\boldsymbol{\psi}^{[-]}) \in \mathrm{image}\left(\boldsymbol{B}_{[n]}\right), \qquad (21)$$

up to integer multiples of 2π. A vector is in the image of a matrix if it is orthogonal to the kernel of the transpose matrix. We thus have the conditions

$$\boldsymbol{C}_{[n+1]}^{\top}\boldsymbol{f}_{[n+1]}(\boldsymbol{\psi}^{[+]}) = 2\pi\boldsymbol{z}^{[+]},$$
$$\boldsymbol{C}_{[n]}\boldsymbol{f}_{[n-1]}(\boldsymbol{\psi}^{[-]}) = 2\pi\boldsymbol{z}^{[-]}, \qquad (22)$$

where $\boldsymbol{z}^{[\pm]}$ is a vector of integers. In the special case where the kernel is parametrized by a single basis vector, $z^{[\pm]}$ is a scalar. In the case of ordinary graphs, the vectors $\boldsymbol{z}^{[\pm]}$ are referred to as winding vectors and its components as winding numbers [7–9]. We will adopt this notation in the following and discuss the interpretation below.

To summarize, we propose the following algorithm to compute phase locked states of the topological Kuramoto model.

Algorithm 1 (Topological nonlinear Kirchhoff conditions). *To compute the phase locked states of the topological Kuramoto model (Eq. (3)):*

1. *Parametrize the set of solutions candidates as (16) while taking into account the constraints $|\boldsymbol{\psi}^{[\pm]}| \leq 1$.*

2. *Choose a partition $S_{[n+1]} = S_{[n+1]}^{\bullet} \cup S_{[n+1]}^{\circ}$ and $S_{[n-1]} = S_{[n-1]}^{\bullet} \cup S_{[n-1]}^{\circ}$.*

3. *Find the solutions of the set of equations (22) where $\boldsymbol{z}^{[\pm]}$ is a vector of integers.*

4. *Check the stability from the Jacobian $\boldsymbol{J}$ if necessary via Eq. (10).*

We briefly discuss three important aspects of this algorithmic approach to phase locking. First, phase locked states with $S^{\circ} = \emptyset$ are always linearly stable (see Sec. III), and as such are especially relevant for applications. States with $S^{\circ} \neq \emptyset$ are typically, but not always unstable. In fact, we will demonstrate the existence of stable phase locked states with $S^{\circ} \neq \emptyset$ close to bifurcations.

Second, the algorithm can be viewed as a topological, nonlinear generalization of Kirchhoff's circuit laws. This is most easily see for the case of ordinary graphs $n = 0$. Here, the entries of $\boldsymbol{K}_{[1]}\boldsymbol{\psi}^{[+]}$ are interpreted as flows or currents defined on edges [48–50]. The set of solution candidates obtained by Eq. (16) correspond to all states that satisfy Kirchhoff's current law at each node. These states can be decomposed into a special solution plus a set of loop flows. If we linearize the sine and arcsine functions and set $\boldsymbol{z}^{[\pm]} = \boldsymbol{0}$, then conditions (22) correspond to Kirchhoff's voltage law. Together, Kirchhoff's voltage and current laws then uniquely determine the currents.

Algorithm 1 introduces two generalizations: (i) The nonlinearity of the sine introduces multistability. Since $\sin(\alpha) = \sin(\alpha + 2\pi z)$ for all $z \in \mathbb{Z}$, we can obtain different values for phase variables when inverting the sine function. Hence, we can obtain different solutions parametrized by the winding numbers z [7–9]. (ii) The

algorithm generalizes the nonlinear Kirchhoff conditions to cell complexes of arbitrary dimensions.

Third, the possible values of the entries of the vectors $z^{[\pm]}$ and thus the number of steady states is bounded. To derive an upper bound, we rewrite Eq. (22) in components and use that $|f_\pm| \leq \pi/2$ and obtain

$$|z_k^{[+]}| = \frac{1}{2\pi} \left| \sum_i C_{[n+1],ik} f_\pm(\psi_i^{[+]}) \right| \leq \frac{1}{4} \sum_i |C_{[n+1],ik}|$$

$$|z_k^{[-]}| = \frac{1}{2\pi} \left| \sum_i C_{[n],ki} f_\pm(\psi_i^{[-]}) \right| \leq \frac{1}{4} \sum_i |C_{[n],ki}|.$$

In the case of normal fixed points with $S^\circ = \emptyset$ we obtain a $<$ instead of the $\leq$.

We recall that the matrices C are closely related to the boundary matrices. We can choose a basis of the kernel such that the kth column of $C_{[n+1]}$ ($C_{[n]}^\top$) is equal to the kth column of $B_{[n+2]}$ ($B_{[n-1]}^\top$) unless k corresponds to the harmonic component. A further simplification is possible by noting that the entries of the boundary matrix have the values $-1, 0, +1$. We then define $m_k^{[+]}$ as the number of non-zero elements of the kth column of $B_{[n+2]}$ and $m_k^{[-]}$ as the number of non-zero elements of the kth row of $B_{[n-1]}$. We then obtain the bounds

$$|z_k^{[+]}| \leq \frac{m_k^{[+]}}{4} \qquad \text{and} \qquad |z_k^{[-]}| \leq \frac{m_k^{[-]}}{4}. \qquad (23)$$

for every k that does not corresponds to the harmonic component. We recall that we obtain a $<$ instead of the $\leq$ for normal fixed points with $S^\circ = \emptyset$. We conclude that we typically need $m_k^{[\pm]} \geq 5$ for multistability.

We finally note that the numbers $m_k^{[\pm]}$ have an intermediate geometric interpretation: The number $m_k^{[+]}$ counts the number of cells of dimension $n+1$ in the boundary of the kth cell of dimension $n+2$. The winding number $z_k^{[+]}$ counts how often the phases $\theta^{[+]}$ wind by 2π when following all cells in this boundary. Likewise, the number $m_k^{[-]}$ counts the number of cells of dimension n that have the kth cell of dimension $n-1$ in its boundary.

V. CLASS 1: POLYGONAL FACES

Polygons are among the simplest models of a cell complex, comprised of a single polygonal face bounded by its edges. We start by considering a ring of 6 vertices, 6 edges and 1 face as illustrated in Fig. 1a. Our main interest here will be dynamics of phases defined on the edges ($n = 1$), which interact via the nodes ($n = 0$) and face ($n = 2$). In this example, we demonstrate our algorithm step-by-step, including the study of unstable states.

Denoting all cells by the vertices in the respective cell,

we have

$$S_{[0]} = \big\{[1], [2], [3], [4], [5], [6]\big\}$$
$$S_{[1]} = \big\{[1, 2], [2, 3], [3, 4], [4, 5], [5, 6], [6, 1]\big\}$$
$$S_{[2]} = \big\{[1, 2, 3, 4, 5, 6]\big\}.$$

The boundary operators are given in Supplementary material. The kernel of the boundary operator $B_{[2]}$ is empty, such that we can write $C_{[2]} = 0$. The kernel of the boundary operator $B_{[1]}^\top$ is spanned by the harmonic vector $\mathbf{1}$, such that $C_{[1]}^\top = \mathbf{1}$. Hence, the set of solutions candidates (16) is given by

$$\psi^{[+]} = \psi_{\rm sp}^{[+]}, \qquad \psi^{[-]} = \psi_{\rm sp}^{[-]} + K_{[1]}^{-1} \mathbf{1} \, \zeta^{[-]}. \qquad (24)$$

The phase conditions (22) reduce to

$$\mathbf{1}^\top f_{[n-1]}(\psi^{[-]}) = 2\pi z^{[-]}. \qquad (25)$$

We start by exploring the fully symmetric case when $\omega = 0$, due to which $\psi^{[+]} = 0$ and $\psi_{\rm sp}^{[-]} = 0$. In Fig. 2 we plot the expression $\mathbf{1}^\top f_{[n-1]}(\psi^{[-]})/(2\pi)$ as a function of the parameter $\zeta^{[-]}$, for each of the partitions $S_{[0]} = S_{[0]}^\bullet \cup S_{[0]}^\circ$. Since there are six elements that can either be $\bullet$ or $\circ$, we obtain 64 different partitions of $S_{[0]}$. Due to symmetry, these 64 curves in Fig. 2 are grouped according to the 7 different multiset permutations (i.e. fixed size of both partitions). Phase locked states are found where the curves cross an integer value. All of the partitions, except those where $|S_{[0]}^\bullet| = |S_{[0]}^\circ| = 3$ provide phase locked solutions for $\omega = 0$. Finally, after checking the stability of each of the phase-locked solutions, we find multistability for the all-normal partition $|S_{[0]}^\bullet| = 6, |S_{[0]}^\circ| = 0$, where three stable solutions coexist. All other solutions are unstable.

Next, we consider the effect of asymmetry in natural frequencies on the existence of solutions, $\omega \neq 0$. Hereby we limit our exploration to two partitions, $S_{[0]}^\circ = \emptyset$, and $S_{[0]}^\circ = [5, 6]$, with $\omega = (0, 0, 0, 0, +\omega_0, -\omega_0)$. We plot the phase conditions (25) divided by 2π as a function of $\zeta^{[-]}$ for chosen ω_0 values in Fig. 3. As before, we find that the former partitioning always gives rise to stable solutions, while the latter typically yields unstable ones. However, near the bifurcation point, the phase-locked state $S_{[0]}^\circ = \emptyset$ becomes $S_{[0]}^\circ = [5, 6]$ without losing stability. Increasing ω_0 further, the stable $S_{[0]}^\circ = [5, 6]$ solution annihilates with another unstable $S_{[0]}^\circ = [5, 6]$ solution in a saddle-node bifurcation. This scenario is shown in the bottom panel of Fig. 3.

Finally, let us generalize our result to polygonal faces of arbitrary size. We consider only the all-normal partitions $S_{[0]}^\bullet = S_{[0]}$ with $\omega = 0$. If the ring size is $s = N_{[0]} = N_{[1]} \geq 3$, the number of stable phased-locked solutions N_{stable} increases with s as

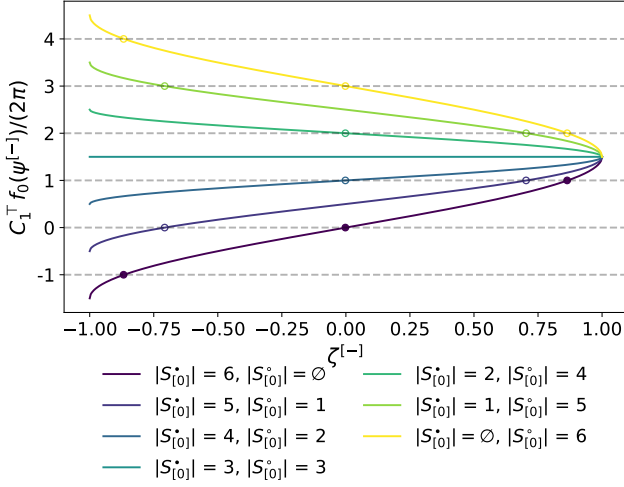$$N_{stable} = 1 + 2 \left\lfloor \frac{s-1}{4} \right\rfloor. \qquad (26)$$

FIG. 2. Phase locked solutions for Example 1. Filled (empty) markers denote stable (unstable) phase locked solutions. Every solution except $|S^\bullet_{[0]}| = |S^\circ_{[0]}| = 3$ intersects an integer multiple of 2π, i.e. has phase locked solutions. For $|S^\bullet_{[0]}| = 6, |S^\circ_{[0]}| = 0$ we find multistability of three phase locked solutions.

This is a consequence of Eq. (23). The solution with $z^{[-]} = 0$ always exists, and other solutions appear in pairs at integer values of $\pm z^{[-]}$, with jumps occurring at $\left|\frac{s-1}{4}\right|$, cf. Fig. 4, in line with previous results on the ordinary Kuramoto model [7].

VI. CLASS 2: PLATONIC SOLIDS

One might wonder what happens when several rings are combined together to create a polyhedron. We therefore now consider another class of elementary cell complexes: convex regular polyhedra in three-dimensional Euclidean space, also known as the Platonic solids. There are exactly five such objects: the tetrahedron, cube, octahedron, dodecahedron, and icosahedron (shown in Fig. 5). We will focus on the $n = 1$ case once again, where the dynamics on edges interacts via nodes and faces, and provide selected results for $n = 0$ and $n = 2$ at the end of the section.

For each cell complex, for $n = 1$, there are $2^{N_{[2]}} \cdot 2^{N_{[0]}}$ partitions of the sets $S_{[2]}$ and $S_{[0]}$. In larger polyhedra, the analysis of all partitions becomes exhaustive. We therefore limit ourselves in this section to the all-normal partition that provides stable normal solutions, $S^\bullet_{[2]} = S_{[2]}, S^\circ_{[2]} = \emptyset$ and $S^\bullet_{[0]} = S_{[0]}, S^\circ_{[0]} = \emptyset$. Moreover, we once again set $\boldsymbol{\omega} = \mathbf{0}$ as our default study case.

We define the cells of the Platonic solids by starting from one initially oriented face, with a fixed vertex order. We then propagate the orientation to neighboring faces by matching shared edges with opposite directions. This way, every face's orientation becomes consistent with its neighbors. The cells $S_{[0]}, S_{[1]}, S_{[2]}$, boundary matrices
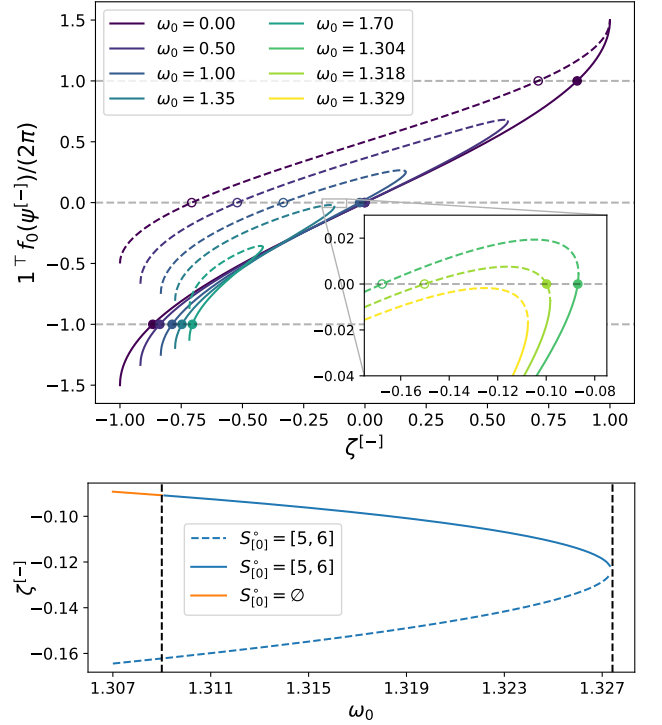

FIG. 3. Top row: Condition (25) for the ring with 6 edges. Solid lines correspond to the partition $S^\circ_{[0]} = \emptyset$, while the dashed to $S^\circ_{[0]} = [5, 6]$, for selected ω_0 values such that $\boldsymbol{\omega} = (0, 0, 0, 0, \omega_0, -\omega_0)$. Empty (filled) markers correspond to linearly unstable (stable) solutions. As ω_0 increases, the number of solutions decreases. The inset shows a curious phenomenon: for a narrow interval of ω_0 values, the solution arising from $S^\circ_{[0]} = [5, 6]$ crosses zero twice, with one solution becoming stable, while $S^\circ_{[0]} = \emptyset$ does not intersect zero. Bottom row: The stable solution $S^\circ_{[0]} = \emptyset$ (orange line) vanishes at around $\omega_0 \approx 1.309$, becoming the stable solution $S^\circ_{[0]} = [5, 6]$. The stable (solid blue line) and unstable solution (dashed blue line) of $S^\circ_{[0]} = [5, 6]$ vanish in a saddle-node bifurcation around $\omega_0 \approx 1.327$.
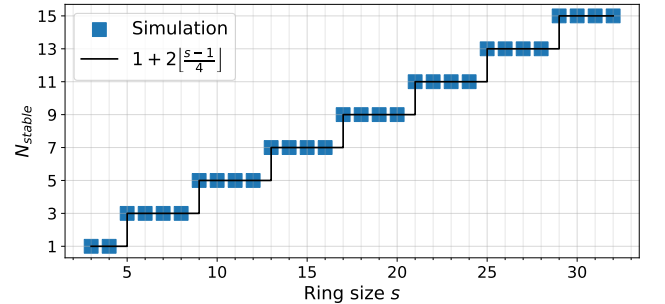

FIG. 4. Number of stable solutions N_{stable} depending on ring size s in an all-normal partitioned ring: comparison of numerical results and Eq. (26).

$\boldsymbol{B}_{[1]}$, $\boldsymbol{B}_{[2]}$ and matrices $\boldsymbol{C}_{[1]}$, $\boldsymbol{C}_{[2]}$ for each Platonic solid are provided in the Supplementary material. Note that according to our definition above, the boundary matrix from face to volume will always be

$$\boldsymbol{B}_{[3]} = \boldsymbol{1} \in \mathbb{R}^{N_{[2]}}$$

Moreover, the C-matrices for $n = 1$ are conveniently given by

$$\boldsymbol{C}_{[1]} = \boldsymbol{1} \in \mathbb{R}^{N_{[0]}}, \qquad \boldsymbol{C}_{[2]}^{\top} = \boldsymbol{1} \in \mathbb{R}^{N_{[2]}},$$

therefore, in the phase conditions,

$$\boldsymbol{1}^{\top} \boldsymbol{f}_{[n+1]}(\boldsymbol{\psi}^{[-]}) = 2\pi z^{[+]}$$
$$\boldsymbol{1}^{\top} \boldsymbol{f}_{[n-1]}(\boldsymbol{\psi}^{[+]}) = 2\pi z^{[-]},$$

$z^{[\pm]}$ are scalars.

Moreover, due to symmetry, the elements of the vectors $\boldsymbol{f}_{[n+1]}(\boldsymbol{\psi}^{[-]})$ and $\boldsymbol{f}_{[n-1]}(\boldsymbol{\psi}^{[+]})$ are the same. For $\boldsymbol{\omega} = 0$, $\boldsymbol{K}_{[n]} = \mathrm{diag}(\boldsymbol{1}_{N_{[0]}})$ and $\boldsymbol{K}_{[n+1]} = \mathrm{diag}(\boldsymbol{1}_{N_{[2]}})$, the set of solution candidates (16) simplifies to

$$\psi^{[+]} = \zeta^{[+]}$$
$$\psi^{[-]} = \zeta^{[-]}$$

Since we only consider the all-normal partitions where the $\boldsymbol{f}$-functions are inverted as arcsin, the phase conditions become

$$N_{[2]} \arcsin \psi^{[+]} = 2\pi z^{[+]}$$
$$N_{[0]} \arcsin \psi^{[-]} = 2\pi z^{[-]}.$$

Hence, we finally obtain

$$\psi^{[+]} = \zeta^{[+]} = \sin\left(\frac{2\pi z^{[+]}}{N_{[2]}}\right),$$
$$\psi^{[-]} = \zeta^{[-]} = \sin\left(\frac{2\pi z^{[-]}}{N_{[0]}}\right).$$

Therefore, the phase-locked states on the edges $n = 1$ are determined by the number of nodes $N_{[0]}$ and faces $N_{[2]}$. We can further take into account the constraints on the winding numbers arising from Eq. (23), such that, analogously to a single ring, the lower dimension will contribute with $N_{St,-}$ possible values of $z^{[-]}$ while the upper with $N_{St,+}$ possible values of $z^{[+]}$

$$N_{St,-} = 1 + 2\left\lfloor \frac{N_{[0]} - 1}{4} \right\rfloor$$
$$N_{St,+} = 1 + 2\left\lfloor \frac{N_{[2]} - 1}{4} \right\rfloor,$$

whereby the Cartesian product of the winding numbers gives all possible solutions of $\psi^{[\pm]}$, and the total number of normal fixed points

$$N_{stable} = N_{St,-} \times N_{St,+}. \tag{27}$$

From this, we immediately see that the tetrahedron with 4 vertices and 4 faces admits only one normal solution since $N_{St,-} = N_{St,+} = 1$. In other words, it is too small to generate multistability.

The larger the objects, the richer the multistability: the remaining four polyhedra admit respectively 9, 9, 45 and 45 coexisting stable solutions, as shown in Fig. 5. The curious result of coinciding numbers of stable solutions arises from the fact that the cube and octahedron, as well as the dodecahedron and icosahedron, are dual polyhedra: each vertex of one corresponds to a face of the other, and each edge connecting two vertices corresponds to the edge connecting the corresponding faces. Consequently, the product from Eq. (27) remains conserved, whereas the states themselves consist of exchanged positions in $(z^{[-]}, z^{[+]})$ or $(\zeta^{[-]}, \zeta^{[+]})$, as can be seen from the examples of the phase-locked solutions of the icosahedron and dodecahedron in the $(\zeta^{[+]}, \zeta^{[-]})$ plane. Thus, objects that belong to the same symmetry group end up with the same universality pattern.

A detailed graphical exploration of the phase locked solutions is shown in Fig. 5. The cascades of multistability inherited from both lower and higher dimensions become larger for larger objects. On the border of the stability region, we find marginally stable states which do not technically belong to the all-normal partition, since they satisfy $\cos\boldsymbol{\theta}^{[-]} = 0$.

Having presented the dynamically homogeneous $\boldsymbol{\omega} = \boldsymbol{0}$ case, let us demonstrate how tuning $\boldsymbol{\omega}$ allows us to control the cascade of multistability. We show this phenomenon on the smallest Platonic solid that admits multiple solutions, the cube. For $\boldsymbol{\omega} = \boldsymbol{0}$, the cube has 9 coexisting solutions (cf. Fig. 5). Upon introducing asymmetry to the vector of natural frequencies $\boldsymbol{\omega} = (0, 0, 0, 0, 0, 0, 0, 0, 0, 0, +\omega_0, -\omega_0)$, the number of stable fixed points decreases gradually, as shown in Fig. 6, disappearing in symmetric pairs or triplets (when a state with the winding number zero is included). In this case, there is no exchange of stability between different partitions as one finds in the ring. States with $S^{\circ} \neq \emptyset$ do not stabilize for any ω_0 value.

We conclude this section with a brief discussion for $n = 0$ and $n = 2$. For the tetrahedron, cube and octahedron, only a single stable solution exists, while for the dodecahedron and icosahedron, calculations become computationally prohibitive due to the combinatorial explosion of the number of possible solutions for winding number vectors. Nevertheless, the simpler cases already demonstrate the importance of including higher-order interactions for multistability in the topological Kuramoto model. Handling the combinatorial explosion poses an interesting problem for future work.

VII. CLASS 3: SIMPLEXES

In contrast to the cell complexes studied earlier, simplexes, especially in low dimensions, are far more lim-
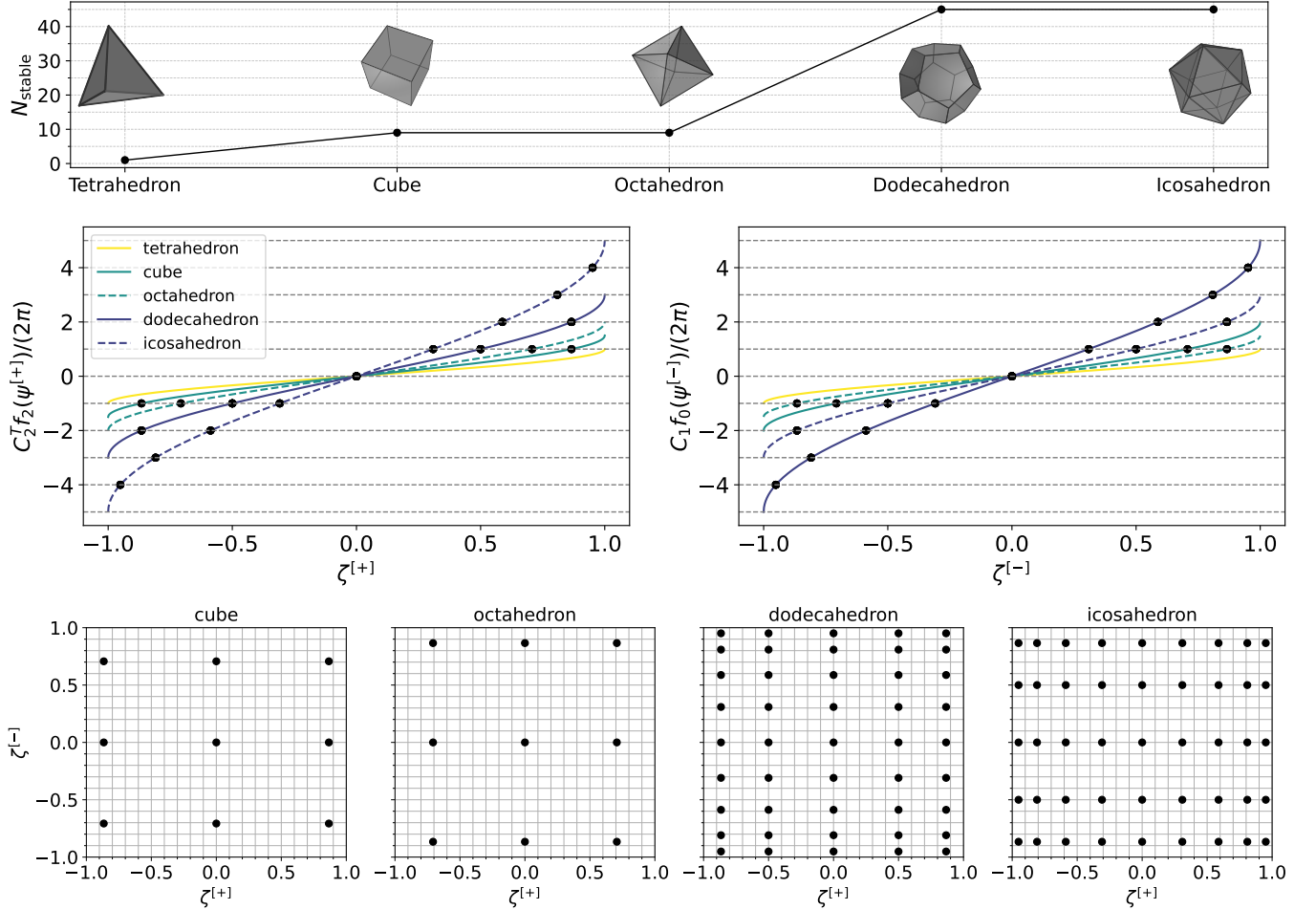
FIG. 5. First row: number of stable phase-locked solutions N_{stable} for each Platonic solid shown in inset. Second row: phase-locked solutions for all Platonic solids. Same colors and different line styles denote dual Platonic solids to emphasize symmetry. Black dots denote stable phase-locked solutions given by Eq. (22). Other than the tetrahedron, all objects exhibit structural multistability cascades where multistability arises due to interactions from both below and above. In the bottom row, we present these solutions in the $(\zeta^{[+]}, \zeta^{[-]})$ plane for the four objects that exhibit multistability.

ited in terms of multistability. The winding number constraint in Eq. (23) tells us that multistability will appear when there are more than 4 cells in the boundary. This is consistent with previously shown results for the 2-simplex (the triangle, or smallest ring, with three edges in the boundary) and 3-simplex (the tetrahedron, also the smallest Platonic solid, with four triangles in its boundary), each admitting only one stable solution for $n = 1$.

Here, we analyze the stable solutions of the all-normal partitions, $S_{[2]}^{\bullet} = S_{[2]}$ and $S_{[0]}^{\bullet} = S_{[0]}$, for all viable n values for simplexes up to 5 dimensions. For definiteness, we once again set $\omega = 0$ and all couplings to unity. Refer to Supplementary material for boundary operators and $\boldsymbol{C}$-matrices for the 4-simplex and 5-simplex. Our results are summarized in Fig. 7. Note that whenever there is one stable solution, it refers to the trivial solution with winding number(s) zero. We list the winding number vectors for all stable solutions in all considered simplexes.

1. **The 2-simplex (triangle)** consists of 3 vertices and 3 edges. It supports the following stable states.

   - For $n = 0$, $z^{[+]} = 0$ with no lower dimension contribution.

   - For $n = 1$, $z^{[-]} = 0$ with no upper dimension contribution.

2. **The 3-simplex (tetrahedron)** consists of 4 vertices, 6 edges and 4 triangular faces, and has been implicitly covered in Sec. VI. It admits single stable states as follows.

   - For $n = 0$, $\boldsymbol{z}^{[+]} = (0, 0, 0)$ with no lower dimension contribution.

   - For $n = 1$, $z^{[-]} = 0$ and $z^{[+]} = 0$.

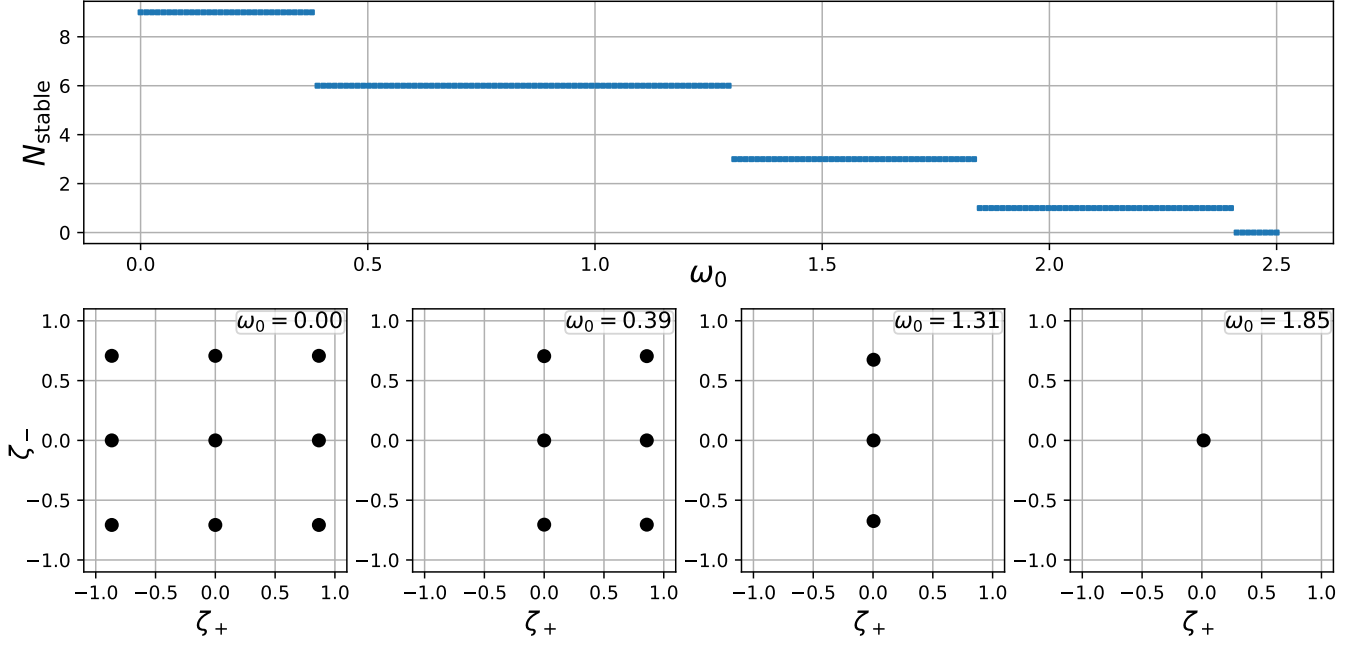   - For $n = 2$, the upper dimension contributes with $\boldsymbol{z}^{[-]} = (0, 0, 0)$.

FIG. 6. Reversal of multistability cascade: gradual decrease of number of stable fixed points in the all-normal partition of the cube by introducing asymmetry to the vector of natural frequencies $\boldsymbol{\omega} = (0, 0, 0, 0, 0, 0, 0, 0, 0, 0, +\omega_0, -\omega_0)$.

FIG. 7. Number of stable phase locked states in simplexes up to dimension 5, for each viable n value.

4. **The 5-simplex** has 6 vertices, 15 edges, 20 triangular faces, 15 tetrahedral cells, and 6 5-cells in its outer boundary. It supports the following stable states.

- For $n = 0$, $\boldsymbol{z}^{[+]} = (0, 0, 0, 0, 0, 0, 0, 0, 0, 0)$.
- For $n = 1$, three solutions coexist: $\boldsymbol{z}^{[+]} = (0, 0, 0, 0, 0, 0, 0, 0, 0, 0)$ with $z^{[-]} \in \{0, \pm 1\}$.
- For $n = 2$, there is only $\boldsymbol{z}^{[+]} = (0, 0, 0, 0, 0)$ with $\boldsymbol{z}^{[-]} = (0, 0, 0, 0, 0)$.
- For $n = 3$, again three solutions coexist, $z^{[+]} \in \{0, \pm 1\}$ with $\boldsymbol{z}^{[-]} = (0, 0, 0, 0, 0, 0, 0, 0, 0, 0)$.
- For $n = 4$, we find only $\boldsymbol{z}^{[-]} = (0, 0, 0, 0, 0, 0, 0, 0, 0, 0)$.

VIII. CONCLUSION AND OUTLOOK

We presented a new framework for identifying phase-locked states of the topological Kuramoto model on arbitrary cell complexes, the topological nonlinear Kirchhoff conditions algorithm. Having applied our algorithm to elementary motifs, namely polygonal faces, Platonic solids, and simplexes, we demonstrated that cell complexes can generate much richer multistability than simplicial complexes of the same dimension.

Essentially, objects need to be large enough to support multistability of solutions. Solutions are characterized by a set of discrete winding numbers associated to cells of lower and higher dimension. We derive explicit bounds on allowed winding numbers, demonstrating that

3. **The 4-simplex (5-cell)** consists of 5 vertices, 10 edges, 10 triangular faces, and 5 tetrahedra. We find the following stable states:

- For $n = 0$, one stable state exists from the upper dimension, $\boldsymbol{z}^{[+]} = (0, 0, 0, 0, 0, 0)$.
- For $n = 1$, the three stable states correspond to $\boldsymbol{z}^{[+]} = (0, 0, 0, 0)$ with $z^{[-]} \in \{0, \pm 1\}$.
- For $n = 2$, three solutions exist with $z^{[+]} \in \{0, \pm 1\}$ and $\boldsymbol{z}^{[-]} = (0, 0, 0, 0)$.
- For $n = 3$, a single solution comes from the lower dimension, with $\boldsymbol{z}^{[-]} = (0, 0, 0, 0, 0, 0)$.

there needs to be more than 4 cells in the boundary for the system to admit multistability. These bounds also explain the emergence of structural cascades of multistability, where multistability is inherited from lower or upper dimensions, or even both. Furthermore, we find indications of universality classes of multistability, where different objects display identical multistability patterns if their upper and lower boundaries share certain characteristics.

Beyond theoretical interest, these results may be interesting for higher-order oscillator networks in a variety of applications. The cell complexes we consider are elementary building blocks for larger complexes, and our method is applicable to any cell complex, and generalizable to models other than the topological Kuramoto model. The concepts of structural cascades and universality classes in multistability may extend to other dynamical processes on higher-order structures, such as diffusion, consensus, or pattern-forming instabilities. Future work could involve studying complexes comprised of these basic building blocks, both in the context of developing more efficient computational algorithms for larger complexes, and applications to real-world phenomena with non-pairwise interactions. Our findings could be relevant to power-grid stability [2, 51], optical and mechanical oscillator arrays [15, 52], neural ensembles [11], and collective decision-making in multi-agent systems [53], among other applications.

Appendix A: Eigenvalues of the Jacobian

Let $\boldsymbol{v} \neq \boldsymbol{0}$ be an eigenvector of the Jacobian matrix $\boldsymbol{J}$ with associated eigenvalue λ such that

$$\boldsymbol{J}\boldsymbol{v} = \lambda\boldsymbol{v}$$
$$\Rightarrow \lambda = \frac{\boldsymbol{v}^\top \boldsymbol{J} \boldsymbol{v}}{\boldsymbol{v}^\top \boldsymbol{v}} .$$

If $\boldsymbol{v}$ is purely harmonic then $\boldsymbol{B}_{[n]}\boldsymbol{v} = \boldsymbol{0}$ and $\boldsymbol{B}_{[n+1]}^\top \boldsymbol{v} = 0$ by definition and thus $\boldsymbol{J}\boldsymbol{v} = \boldsymbol{0} \Rightarrow \lambda = 0$. If $\boldsymbol{v}$ is not purely harmonic then $\boldsymbol{y}^{[-]} = \boldsymbol{B}_{[n]}\boldsymbol{v} \neq 0$ or/and $\boldsymbol{y}^{[+]} = \boldsymbol{B}_{[n+1]}^\top \boldsymbol{v} \neq 0$. We thus obtain

$$\lambda = -(\boldsymbol{v}^\top \boldsymbol{v})^{-1} \bigg\{ \boldsymbol{y}^{[-]\top} \boldsymbol{K}_{[n]} \mathrm{diag}\left[\cos\left(\bar{\boldsymbol{\theta}}^{[-]} \right) \right] \boldsymbol{y}^{[-]}$$
$$+ \boldsymbol{y}^{[+]\top} \boldsymbol{K}_{[n+1]} \mathrm{diag}\left[\cos\left(\bar{\boldsymbol{\theta}}^{[+]} \right) \right] \boldsymbol{y}^{[+]} \bigg\}$$
$$= -(\boldsymbol{v}^\top \boldsymbol{v})^{-1} \bigg\{ \sum_j \left(y_j^{[-]} \right)^2 (K_{[n]})_{jj} \cos\left(\bar{\theta}_j^{[-]} \right)$$
$$+ \sum_j \left(y_j^{[+]} \right)^2 (K_{[n+1]})_{jj} \cos\left(\bar{\theta}_j^{[+]} \right) \bigg\}.$$

If the stationary state satisfies the conditions in Eq. (11), this implies

$$\lambda < 0.$$

[1] A. Pikovsky, M. Rosenblum, and J. Kurths, *Synchronization: A Universal Concept in Nonlinear Sciences* (Cambridge University Press, 2001).

[2] F. Dörfler and F. Bullo, Synchronization in complex networks of phase oscillators: A survey, Automatica **50**, 1539 (2014).

[3] Y. Kuramoto, Self-entrainment of a population of coupled non-linear oscillators, in *International symposium on mathematical problems in theoretical physics: January 23–29, 1975, kyoto university, kyoto/Japan* (Springer, 1975) pp. 420–422.

[4] J. A. Acebrón, L. L. Bonilla, C. J. Pérez Vicente, F. Ritort, and R. Spigler, The kuramoto model: A simple paradigm for synchronization phenomena, Reviews of modern physics **77**, 137 (2005).

[5] S. H. Strogatz, From kuramoto to crawford: exploring the onset of synchronization in populations of coupled oscillators, Physica D: Nonlinear Phenomena **143**, 1 (2000).

[6] F. A. Rodrigues, T. K. D. Peron, P. Ji, and J. Kurths, The kuramoto model in complex networks, Physics Reports **610**, 1 (2016).

[7] D. Manik, M. Timme, and D. Witthaut, Cycle flows and multistability in oscillatory networks, Chaos: An Interdisciplinary Journal of Nonlinear Science **27** (2017).

[8] R. Delabays, T. Coletta, and P. Jacquod, Multistability of phase-locking and topological winding numbers in locally coupled kuramoto models on single-loop networks, Journal of Mathematical Physics **57** (2016).

[9] S. Jafarpour, E. Y. Huang, K. D. Smith, and F. Bullo, Flow and elastic networks on the n-torus: Geometry, analysis, and computation, SIAM Review **64**, 59 (2022).

[10] F. Hellmann, P. Schultz, P. Jaros, R. Levchenko, T. Kapitaniak, J. Kurths, and Y. Maistrenko, Network-induced multistability through lossy coupling and exotic solitary states, Nature communications **11**, 592 (2020).

[11] M. Breakspear, S. Heitmann, and A. Daffertshofer, Generative models of cortical oscillations: neurobiological implications of the Kuramoto model, Frontiers in Human Neuroscience **4**, 190 (2010).

[12] A. E. Sizemore, J. E. Phillips-Cremins, R. Ghrist, and D. S. Bassett, Cliques and cavities in the human connectome, Journal of Computational Neuroscience **44**, 115 (2018).

[13] C. Giusti, R. Ghrist, and D. S. Bassett, Two's company, three (or more) is a simplex: Algebraic-topological tools for understanding higher-order structure in neural data, Journal of Computational Neuroscience **41**, 1 (2016).

[14] M. Andjelković, B. Tadić, and R. Melnik, The topology of higher-order complexes associated with brain hubs in human connectomes, Scientific Reports **10**, 17320 (2020).

[15] M. Nixon, E. Ronen, A. A. Friesem, and N. Davidson, Observing geometric frustration with thousands of coupled lasers, Physical Review Letters **110**, 184102 (2013).

[16] E. Estrada and G. J. Ross, Centralities in simplicial complexes. applications to protein interaction networks, Journal of Theoretical Biology **438**, 46 (2018).

[17] A. P. Millán, H. Sun, L. Giambagli, R. Muolo, T. Carletti, J. J. Torres, F. Radicchi, J. Kurths, and G. Bianconi, Topology shapes dynamics of higher-order networks, Nature Physics **21**, 353 (2025).

[18] F. Battiston, G. Cencetti, I. Iacopini, V. Latora, M. Lucas, A. Patania, J.-G. Young, and G. Petri, Networks beyond pairwise interactions: Structure and dynamics, Physics reports **874**, 1 (2020).

[19] F. Battiston, E. Amico, A. Barrat, G. Bianconi, G. Ferraz de Arruda, B. Franceschiello, I. Iacopini, S. Kéfi, V. Latora, Y. Moreno, *et al.*, The physics of higher-order interactions in complex systems, Nature Physics **17**, 1093 (2021).

[20] G. Bianconi, *Higher-Order Networks: An Introduction to Simplicial Complexes* (Cambridge University Press, 2021).

[21] L. Torres, G. Bianconi, *et al.*, The hidden geometry of higher-order networks, Nature Communications **12**, 286 (2021).

[22] C. Bick, T. Gross, H. A. Harrington, and M. T. Schaub, What are higher-order networks?, SIAM Review **65**, 686 (2023).

[23] D. Horak, S. Maletić, and M. Rajković, Persistent homology of complex networks, Journal of Statistical Mechanics: Theory and Experiment **2009**, P03034 (2009).

[24] G. Petri, M. Scolamiero, I. Donato, and F. Vaccarino, Topological strata of weighted complex networks, PLoS One **8**, e66506 (2013).

[25] G. Petri, P. Expert, F. Turkheimer, R. L. Carhart-Harris, D. Nutt, P. J. Hellyer, and F. Vaccarino, Homological scaffolds of brain functional networks, Journal of The Royal Society Interface **11**, 20140873 (2014).

[26] Z. Wu, G. Menichetti, C. Rahmede, and G. Bianconi, Emergent complex network geometry, Scientific Reports **5**, 10073 (2015).

[27] I. Iacopini, G. Petri, A. Barrat, and V. Latora, Simplicial models of social contagion, Nature Communications **10**, 2485 (2019).

[28] M. Andjelković, B. Tadić, M. Mitrović Dankulov, M. Rajković, and R. Melnik, Topology of innovation spaces in the knowledge networks emerging through questions-and-answers, PLOS ONE **11**, e0154655 (2016).

[29] A. P. Millán, J. J. Torres, and G. Bianconi, Explosive higher-order kuramoto dynamics on simplicial complexes, Physical Review Letters **124**, 218301 (2020).

[30] A. P. Millán, J. J. Torres, and G. Bianconi, Synchronization in simplicial complexes of phase oscillators, Chaos **31**, 033122 (2021).

[31] R. Ghorbanchian, J. G. Restrepo, J. J. Torres, and G. Bianconi, Higher-order simplicial synchronization of coupled topological signals, Communications Physics **4**, 120 (2021).

[32] M. Nurisso, A. Arnaudon, M. Lucas, R. L. Peach, P. Expert, F. Vaccarino, and G. Petri, A unified framework for simplicial kuramoto models, Chaos **34**, 053118 (2024).

[33] P. S. Skardal and A. Arenas, Higher order interactions in complex networks of phase oscillators promote abrupt synchronization switching, Communications Physics **3**, 218 (2020).

[34] M. Lucas, G. Cencetti, and F. Battiston, Multiorder laplacian for synchronization in higher-order networks, Physical Review Research **2**, 033410 (2020).

[35] R. Ghorbanchian, G. Bianconi, and F. Radicchi, Topological obstructions to synchronization in simplicial complexes, Physical Review E **103**, 022304 (2021).

[36] T. Carletti, L. Giambagli, and G. Bianconi, Global topological synchronization on simplicial and cell complexes, Physical review letters **130**, 187401 (2023).

[37] P. S. Skardal and A. Arenas, Abrupt desynchronization and extensive multistability in globally coupled oscillator simplexes, Physical Review Letters **122**, 248301 (2019).

[38] L. DeVille, Consensus on simplicial complexes: Results on stability and synchronization, Chaos **31**, 023137 (2021).

[39] L. V. Gambuzza, F. D. Patti, L. Gallo, S. Lepri, M. Romance, R. Criado, M. Frasca, V. Latora, and S. Boccaletti, Stability of synchronization in simplicial complexes, Nature Communications **12**, 1255 (2021).

[40] F. Parastesh, M. Mehrabbeik, K. Rajagopal, S. Jafari, M. Perc, C. I. del Genio, and S. Boccaletti, Synchronization stability in simplicial complexes of near-identical systems, Physical Review Research **7**, 033039 (2025).

[41] J. Hoppe, V. P. Grande, and M. T. Schaub, Don't be afraid of cell complexes! an introduction from an applied perspective, arXiv preprint arXiv:2506.09726 (2025).

[42] T. M. Roddenberry, M. T. Schaub, and M. Hajij, Signal processing on cell complexes, in *IEEE International Conference on Acoustics, Speech and Signal Processing (ICASSP)* (2022) pp. 8852–8856.

[43] L. Giambagli, L. Calmon, R. Muolo, T. Carletti, and G. Bianconi, Diffusion-driven instability of topological signals coupled by the dirac operator, Physical Review E **106**, 064314 (2022).

[44] D. Mulder and G. Bianconi, Network geometry and complexity, Journal of Statistical Physics **173**, 783 (2018).

[45] S. Barbarossa and S. Sardellitti, Topological signal processing over simplicial complexes, IEEE Transactions on Signal Processing **68**, 2992 (2020).

[46] S. H. Strogatz, *Nonlinear dynamics and chaos with student solutions manual: With applications to physics, biology, chemistry, and engineering* (CRC press, 2018).

[47] D. Manik, D. Witthaut, B. Schäfer, M. Matthiae, A. Sorge, M. Rohden, E. Katifori, and M. Timme, Supply networks: Instabilities without overload, The European Physical Journal Special Topics **223**, 2527 (2014).

[48] C. Hartmann, P. C. Böttcher, D. Gross, and D. Witthaut, Synchronized states of power grids and oscillator networks by convex optimization, PRX energy **3**, 043004 (2024).

[49] I. Bačić, C. Hartmann, P. C. Böttcher, D. Gross, A. Benigni, and D. Witthaut, Existence of phase-cohesive solutions of the lossless power-flow equations, Preprint, TechRxiv (2025).

[50] A. Parameswaran, I. Bačić, A. Benigni, and D. Witthaut, Symmetry breaking in minimum dissipation networks, Preprint, arXiv (2025).

[51] A. E. Motter, S. A. Myers, M. Anghel, and T. Nishikawa, Spontaneous synchrony in power-grid networks, Nature Physics **9**, 191 (2013).

[52] M. Zhang, G. S. Wiederhecker, S. Manipatruni, A. Barnard, P. McEuen, and M. Lipson, Synchronization of micromechanical oscillators using light, Physical Review Letters **109**, 233906 (2012).

[53] R. Olfati-Saber, J. A. Fax, and R. M. Murray, Consensus and cooperation in networked multi-agent systems, Proceedings of the IEEE **95**, 215 (2007).